An Optimal Fast-Charging Strategy for Lithium-Ion Batteries via an Electrochemical–Thermal Model with Intercalation-Induced Stresses and Film Growth

Guangwei Chen[ID]**, Zhitao Liu** *[ID] **and Hongye Su**

State Key Laboratory of Industrial Control Technology, Institute of Cyber-Systems and Control,
Zhejiang University, Hangzhou 310027, China; gwchen@zju.edu.cn (G.C.); hysu@iipc.zju.edu.cn (H.S.)
* Correspondence: ztliu@zju.edu.cn; Tel.: +86-0571-87952233 (ext. 8239)

Abstract: Optimal fast charging is an important factor in battery management systems (BMS). Traditional charging strategies for lithium-ion batteries, such as the constant current–constant voltage (CC–CV) pattern, do not take capacity aging mechanisms into account, which are not only disadvantageous in the life-time usage of the batteries, but also unsafe. In this paper, we employ the dynamic optimization (DP) method to achieve the optimal charging current curve for a lithium-ion battery by introducing limits on the intercalation-induced stresses and the solid–liquid interface film growth based on an electrochemical–thermal model. Furthermore, the backstepping technique is utilized to control the temperature to avoid overheating. This paper concentrates on solving the issue of minimizing charging time in a given target State of Charge (SoC), while limiting the capacity loss caused by intercalation-induced stresses and film formation. The results indicate that the proposed optimal charging method in this paper offers a good compromise between the charging time and battery aging.

1. Introduction

Lithium-ion batteries have been used in many electronic products due to their high cell voltage, high energy density, high power density, convenient operating temperature range, lack of memory property, and high cycle life [1]. When operating a lithium-ion battery efficiently and safely during charging, long charging time, capacity degradation, capacity wastage, and overheating are the main difficulties that need to be overcome.

In recent years, many researchers have made efforts to optimize lithium battery charging. Many results are based on traditional charging patterns, such as the constant-current (CC) pattern and the constant current–constant voltage (CC–CV) pattern, without considering the aging process. For example, Liu and Luo [2] proposed a Taguchi-based algorithm and adopted orthogonal arrays to obtain the optimal rapid-charging strategy for a piecewise CC charging approach, which can charge a battery cell from 0% to 75% within 40 min and increase the cycle life by more than 60%. On the basis of the open circuit voltage (OCV)-resistance equivalent circuit model, Abdollahi et al. [3] presented a closed-form solution for optimally charging a lithium-ion battery; the target function is established through a combination of two consumption functions: time-to-charge (TTC) and energy losses (EL). Here, the CC–CV pattern is selected as the optimal charging scheme, where the current in the CC stage is a function of the ratio of weighting on TTC and EL. Then, Abdollahi et al. [4] proposed the objective function consisting of TTC, EL, and a temperature rise index (TRI). Then, the value of the current in the CC stage is also considered as a function of the ratio of weighting on TTC and EL,

and finally the analytical solution for the optimal problem is derived. Monem et al. [5] studied the influence of three charging strategies including CC, CC–CV, and constant current–constant voltage with negative pulse (CC–CVNP) on the battery's cycle life. The results show that the CC–CVNP pattern with low amplitude and less negative pulses is more efficient than the CC and CC–CV patterns. Liu et al. [6] firstly put forward a triple-objective function for optimal battery charging on the basis of a coupled thermoelectric model. Then, the CC–CV charge strategy is optimized, which offers the best compromise among three significant performance indexes consisting of charging time, energy loss, and temperature rise. Fang et al. [7] permit users to specify charging objectives and reach them by dynamic optimal control for the first time and proposed two charging methods based on the linear quadratic control theory without real-time constrained optimization computation. Compared to the conventional open-loop regulation of fast charging, the close-loop optimal method can be used to accurately control the specific parameters, such as temperature, current, and voltage. Patnaik et al. [8] came up with a constant temperature–constant voltage (CT-CV) charging algorithm that considers battery temperature as a key feedback variable. Then, a simple and easy-to-realize proportional-integral-derivative (PID) controller is employed to implement this close-loop method and the results indicate that the proposed approach achieved a 20% faster charging rate with an identical total temperature increase as compared to the constant current–constant voltage (CC–CV) technique. Klein et al. [9] paid attention to minimum charging time and proposed a simple one-step predictive control algorithm that is capable of solving the time-optimal solution and satisfying the real-time requirement. On the basis of the electrochemical battery model, Pramanik et al. [10] introduced a novel method for optimally charging the lithium-ion battery cell, which establishes the objective function aiming to minimize the charging cost. The result indicates that the optimal charging method presented in the paper [10] can decrease the charging time of a lithium-ion cell, meanwhile guaranteeing the temperature limit when compared with the traditional constant current charging. Considering the electrolyte and thermal dynamics based on a single particle model, the Legendre–Gauss–Radau (LGR) pseudo-spectral approach is used to solve the problem of nonlinear multistate optimal control, and the minimum time charge strategies are analyzed minutely while taking the solid and electrolyte phase concentration limits and temperature constraint into account [11].

Generally speaking, fast charging can accelerate the battery aging processes. For reducing the aging rate, some researchers consider the aging process when optimizing the fast-charging strategy and some good results have been obtained. For example, through coupling incremental capacity (IC) and IC peak area analysis with the mechanistic model, Ansean et al. [12] quantified the mechanism of degradation that leads to the aging of the battery cell. In addition, the results show that aging is caused by a loss of lithium ions and a lower level of loss of active material on the negative electrode. On the basis of cycle-life testing (up to 4500 cycles), Ansean et al. [13] proposed a multistage fast-charging algorithm which allows a full recharging of the cell (0% to 100% SoC) within 20 min (indeed after 4500 cycles are reached) and does not cause any remarkable degradation to the battery cell. Considering the influence of intercalation-induced stress on aging, Suthar et al. [14] used dynamic optimization to achieve the optimal current profile to fast charge a lithium-ion battery through a single-particle model while coupling this with the intercalation-induced stress generation model. In addition, this was the first time protocols for optimally charging batteries while ensuring a minimal mechanical cost to the electrode particles during intercalation were demonstrated. Torchio et al. [15] used the first-principles pseudo-two-dimensional (P2D) model together with the capacity fade mechanisms that work when the battery is operating. Then, the model predictive control (MPC) method based on a linearized model of the P2D model was proposed to approach a target value of the state of charge (SoC) while considering the degradation process of the system as well as the thermal and voltage limits. To analyze the effect of static and dynamic fast-charging current strategies on the degradation properties of lithium-ion batteries, Monem et al. [16] applied both the static and dynamic fast-charging current profiles to a lithium-ion battery cell. After 1700 cycles, the result shows that the dynamic fast-charging current profile had a more outstanding role in reducing the aging rate and the charging time of

cells than the static fast-charging profile. To reduce the influence of fast charging on battery aging, Ali et al. [17] proposed a temperature control method based on fuzzy logic that protects the batteries from overvoltage and overheating. The result illustrates that the proposed fast-charging pattern spends 9.76% less time during full battery recharging than the conventional CC–CV method, and the approach does not bring significant degradation. As a compromise between the three objectives of high safety, longer lifetime, and a lower charging time, Zou et al. [18] proposed a fast-charging method on the basis of the electrochemical model and MPC theory. Here, the battery optimal charging issue is described in a linear time-varying model for the implementation of the MPC algorithm. Similarly, Lina et al. [19] presented an electrolyte enhanced single particle model with aging mechanisms which considers the effect of electrolyte dynamics, then the dynamic programming DP approach is adopted to obtain the optimal charging profiles to reduce the charge time and battery aging. On the basis of the electrochemical–thermal capacity fade model, Xu et al. [20] used the DP optimization algorithm to minimize capacity fade, temperature rise, and charging time. Although there are many papers considering the aging process in terms of optimizing the fast charge curve, the aging models used in the above-mentioned papers seldom involve intrinsic aging mechanisms and never consider the effects of intercalation-induced stress and film growth together on the aging process.

In this paper, the electrochemical–thermal model is employed to obtain the optimal charging profile and control the temperature of cell. Controlling the temperature of the hottest point inside the cell based on the backstepping method can help avoid overheating. During fast charging, intercalation-induced stress will cause particle fracture which can accelerate the aging process. Hence, restricting intercalation-induced stress to a given range is significant to reduce the degradation of cells when seeking the optimal fast-charging profile. Furthermore, the main aging cause is the growth of film on the surface of particles, and this film is a compound containing lithium which cannot be reused. Therefore, confining the growth rate of surficial film to a proper range can maximize the available lithium, which is another contribution of this paper. To sum up, on the basis of maintaining a constant temperature using the backstepping control method and minimizing the charging time while limiting intercalation-induced stress and the film growth to an appropriate range are the main contributions of this paper.

2. Electrochemical–Thermal Model with Intercalation-Induced Stress and Film Growth

2.1. SPM-Electrolyte-T Model

The SPM-Electrolyte-T Model is a simplified version of the first principle electrochemical model of batteries composed of a single particle model, electrolyte dynamics, and thermal dynamics. Considering the effects of electrolyte and thermal dynamics can help us investigate the fast-charging scheme to reduce battery aging to prolong the lifetime of lithium-ion batteries. The single particle model can be described by the following partial differential equation [21]:

$$\frac{\partial c_s^\pm}{\partial t} = D_s^\pm(T_{avg}) \times \left(\frac{\partial^2 c_s^\pm}{\partial r^2} + \frac{2}{r} \frac{\partial c_s^\pm}{\partial r} \right) \tag{1}$$

with the following conditions:

$$\frac{\partial c_s^\pm}{\partial r}(0,t) = 0, \frac{\partial c_s^\pm}{\partial r}(R_s^\pm,t) = \frac{\pm I(t)}{Fa^\pm AL^\pm} \tag{2}$$

The definitions of the relevant electrochemical parameters are listed in the attached table.

Most studies relevant to the electrochemical model of lithium-ion batteries ignore the influence of electrolyte dynamics for inexpensive computation. However, when the charging or discharging current is high, there would be a remarkable electrolyte concentration potential between the cathode and the anode, which has a significant impact on the prediction of the terminal voltage. Specifically, the process of fast charging requires more than a 2 C current, which has enough power to produce an

obvious concentration potential. Hence, during the operation of fast charging, it is wise to consider electrolyte dynamics.

The electrolyte dynamics are governed by

$$\varepsilon_e^{\pm} \frac{\partial c_e^{\pm}}{\partial t}(x,t) = \frac{\partial}{\partial x}\left[D_e^{eff}\left(c_e^{\pm}, T_{avg}\right)\frac{\partial c_e^{\pm}}{\partial x}(x,t)\right] \mp \frac{\left(1 - t_c^0\right)I(t)}{FAL^{\pm}} \tag{3}$$

$$\varepsilon_e^{sep} \frac{\partial c_e^{sep}}{\partial t}(x,t) = \frac{\partial}{\partial x}\left[D_e^{eff}\left(c_e^{sep}, T_{avg}\right)\frac{\partial c_e^{sep}}{\partial x}(x,t)\right] \tag{4}$$

with the boundary conditions

$$\frac{\partial c_e^-}{\partial x}(0^-,t) = \frac{\partial c_e^+}{\partial x}(0^+,t) = 0 \tag{5}$$

$$D_e^{eff}\left(L^-, T_{avg}\right)\frac{\partial c_e^-}{\partial x}(L^-,t) = D_e^{eff}\left(0^{sep}, T_{avg}\right) \times \frac{\partial c_e^{sep}}{\partial x}(0^{sep},t) \tag{6}$$

$$D_e^{eff}\left(L^{sep}, T_{avg}\right)\frac{\partial c_e^{sep}}{\partial x}(L^{sep},t) = D_e^{eff}\left(L^+, T_{avg}\right) \times \frac{\partial c_e^+}{\partial x}(L^+,t) \tag{7}$$

$$c_e(L^-,t) = c_e(0^{sep},t), \quad c_e(L^{sep},t) = c_e\left(L^+,t\right) \tag{8}$$

where $D_e^{eff}(c_e, T_{avg}) = D_e(c_e, T_{avg})(c_e) \cdot (\varepsilon_e)^{brug}$ is the effective electrolyte diffusivity, which means that the diffusion rate of lithium ions is related to its concentration and temperature; t_c^0 is the transference number, which is deemed to be constant; $\varepsilon_e^+, \varepsilon_e^-, \varepsilon_e^{sep}$ are the volume fractions of the electrolyte in the cathode, anode, and separator, respectively, and L^+, L^-, L^{sep} are the lengths of the cathode, anode, and separator. The effects of electrolyte dynamics on the terminal voltage equation is presented as follows, considering:

$$\begin{aligned} V(t) = \quad & \frac{RT_{avg}(t)}{\alpha F}\sinh^{-1}\left(\frac{I(t)}{2a^+AL^+i_0^+(t)}\right) - \frac{RT_{avg}(t)}{\alpha F}\sinh^{-1}\left(\frac{-I(t)}{2a^-AL^-i_0^-(t)}\right) \\ & + U^+\left(c_{ss}^+(t)\right) - U^-\left(c_{ss}^-(t)\right) + \left(\frac{R_f^+}{a^+AL^+} + \frac{R_f^-}{a^-AL^-} + \frac{R_{ce}\left(T_{avg}(t)\right)}{A}\right)I(t) \\ & + \left(\frac{L^+ + 2L^{sep} + L^-}{2A\overline{\kappa}^{eff}\left(T_{avg}\right)}\right)I(t) + k_{conc}(t)\left[\ln c_e(0^+,t) - \ln c_e(0^-,t)\right] \end{aligned} \tag{9}$$

where

$$i_0^{\pm}(t) = k^{\pm}\left(T_{avg}\right)[c_{ss}^{\pm}(t)]^{\alpha_c}\left[c_e^{\pm}(x,t)\left(c_{s,\max}^{\pm} - c_{ss}^{\pm}(t)\right)\right]^{\alpha_a} \tag{10}$$

Most model parameters of battery cells are relative to the temperature and are expressed by the following equation:

$$P\left(T_{avg}\right) = P_0 \exp\left(\frac{E_{a_P}}{R}\left(\frac{1}{T_0} - \frac{1}{T_{avg}}\right)\right) \tag{11}$$

where P_0 is the parameter when the temperature is equal to T_0; and E_{a_P} is the activation energy of parameter P. The average temperature T_{avg} can be obtained by the following equations:

$$\frac{\partial T(r_1,t)}{\partial t}\frac{1}{\alpha} = \frac{\partial T^2(r_1,t)}{\partial r_1^2} + \frac{1}{r_1}\frac{\partial T(r_1,t)}{\partial r_1} + \frac{\dot{q}}{k} \tag{12}$$

$$T_{avg}(t) = \frac{1}{r_1}\int_0^{r_1} T(s,t)ds \tag{13}$$

with the boundary conditions

$$\frac{\partial T(0,t)}{\partial r_1} = 0, \frac{\partial T(R_b,t)}{\partial r_1} = U = \frac{h}{k}(T_a - T(R_b,t)) \tag{14}$$

where $r \in [0, R_b]$ is the radial coordinate of a cylindrical battery; $\alpha = k/(\rho C_p)$ is proportional to the average thermal conductivity k; ρ is the average mass density and C_p is the average specific thermal capacity; $\dot{q}$ is the volumetric heat generated rate; and T_a is the ambient temperature. $\dot{q}$ can be computed by the following equation:

$$\dot{q} = I(t) \times \left(U_o(t) - U_{ter} - \overline{T}(t) \frac{\partial U_o(t)}{\partial \overline{T}(t)} \right) \tag{15}$$

where $U_o(t)$ is the open circuit voltage, which is a function of the boundary concentration; $U_{ter} = V(t)$ is the terminal voltage; and $\partial U_o(t)/\partial \overline{T}(t)$ is the entropic heat generation which is too small to neglect. The open circuit voltage $U_o(t)$ can be given by the following equation:

$$U_o(t) = U^+(c_{ss}^+(t)) - U^-(c_{ss}^-(t)) \tag{16}$$

Then, the volumetric heat generated rate $\dot{q}$ can be rewritten as follows:

$$
\begin{aligned}
\dot{q} = I(t) \times (U_o(t) - V(t)) = I(t) \times \Bigg\{ & \frac{RT_{avg}(t)}{\alpha F} \sinh^{-1}\left(\frac{I(t)}{2a^+ AL^+ i_0^{-+}(t)} \right) \\
& - \frac{RT_{avg}(t)}{\alpha F} \sinh^{-1}\left(\frac{-I(t)}{2a^- AL^- i_0^-(t)} \right) + \left(\frac{R_f^+}{a^+ AL^+} + \frac{R_f^-}{a^- AL^-} + \frac{R_{ce}(T_{avg}(t))}{A} \right) I(t) \\
& + \left(\frac{L^+ + 2L^{sep} + L^-}{2A\overline{\kappa}^{eff}(T_{avg})} \right) I(t) + k_{conc}(t) [\ln c_e(0^+, t) - \ln c_e(0^-, t)] \Bigg\}
\end{aligned}
\tag{17}
$$

2.2. Intercalation-Induced Stress

The intercalation-induced stress generated by lithium-ion intercalation and deintercalation influences the diffusion of lithium and even causes electrode particle fracture. This electrode particle fracture will accelerate aging. Considering the effects of intercalation-induced stress helps us to investigate the fast-charging scheme to reduce the electrode particle fracture and thus prolong the lifetime of the lithium-ion battery. The intercalation-induced stresses are composed of radial stress σ_r and tangential stress σ_t, which are dependent of the lithium concentration [22]:

$$
\begin{aligned}
\sigma_r^\pm(r, t) &= 2\beta^\pm \left[\frac{1}{\left(R_s^j\right)^3} \int_0^{R_s^\pm} \widetilde{c}_s^\pm r^2 dr - \frac{1}{r^3} \int_0^r \widetilde{c}_s^\pm \rho^2 d\rho \right] \\
\sigma_t^\pm(r, t) &= \beta^\pm \left[\frac{2}{\left(R_s^j\right)^3} \int_0^{R_s^\pm} \widetilde{c}_s^\pm r^2 dr + \frac{1}{r^3} \int_0^r \widetilde{c}_s^\pm \rho^2 d\rho - \widetilde{c}_s^\pm \right]
\end{aligned}
\tag{18}
$$

where, $\beta^\pm = \Omega^\pm E^\pm / 3(1 - v^\pm)$. $\Omega^\pm$, $E^\pm$, and $v^\pm$ are the partial molar volume, Young's Modulus, and Poisson's ratio of the electrode material in the cathode and anode, respectively, which have different sensitivities to temperature. $\widetilde{c}^\pm$ is the concentration change from the stress-free value. The resultant stress is a weighted sum of σ_r and σ_t:

$$\sigma_{res}^\pm = \frac{\sigma_r^\pm + 2\sigma_t^\pm}{3} = \frac{2}{3}\beta^\pm \left[\frac{3}{(R_s^\pm)^3} \int_0^{R_s^\pm} \widetilde{c}_s^\pm r^2 dr - \widetilde{c}_s^\pm \right] \tag{19}$$

From [23], we know that the maximum absolute values of radial and tangential stress are located at the center and the surface of the particle, respectively. Taking the anode as an example, we have

$$
\begin{aligned}
\sigma_{r,\max}^-(t) &= 2\beta^- \left[\frac{1}{(R_s^-)^3} \int_0^{R_s^-} \widetilde{c}_s^- r^2 dr - \frac{1}{3}\widetilde{c}_s^-(0, t) \right] \\
\sigma_{t,\max}^-(t) &= \beta^- \left[\frac{3}{(R_s^-)^3} \int_0^{R_s^-} \widetilde{c}_s^- r^2 dr - \widetilde{c}_s^-(R_s^-, t) \right]
\end{aligned}
\tag{20}
$$

According to Equation (19), we find that the maximum value of the resultant stress is located at the point where the lithium concentration is the minimum value of the electrode particle. That is

$$\sigma_{res,max}^{-} = \frac{2}{3}\beta^{-}\left[\frac{3}{(R_s^{-})^3}\int_0^{R_s^{-}}\widetilde{c_s^{-}}\,r^2 dr - \widetilde{c}_{s,min}^{-}\right] \tag{21}$$

Figure 1 shows the input current under Urban Dynamometer Driving Schedule (UDDS), which is applied to a battery cell. Then, the maximum absolute values of radial stress, tangential stress, and the resultant stresses are investigated. According to Equation (21), the intercalation-induced stresses are caused by the lithium-ion concentration nonuniformity in space, which is related to the values of the charging and discharging current. When the current is positive, the lithium-ion concentration in the surface of the particle is smaller than in the center of the particle, that is, the maximum radical stress is positive and the maximum tangential stress is negative, and vice versa. From the input current under UDDS, we know that the current is rapidly changing, which can cause the oscillation of lithium-ion concentration and enlarge the imbalance of lithium-ion concentration in space. Hence, the maximum absolute values of radial stress, tangential stress, and the resultant stresses change rapidly over time, as shown in Figures 2–4. From the three figures, we can see that when the input current is negative, the absolute values of the three stresses will increase gradually, and vice versa. This is because the negative current increases the lithium-ion concentration nonuniformity in space and the positive current decreases this nonuniformity. Besides that, we can find that the absolute values of the three stresses have the same changing curve, which agrees with Equations (20) and (21). Another finding is that the value of the maximum tangential stress is larger than the maximum resultant stress, and the maximum resultant stress is always larger than the maximum radial stress. Hence, by adjusting the input current, the radial stress, tangential stress, and the resultant stress can be controlled to decrease the aging of a battery cell.
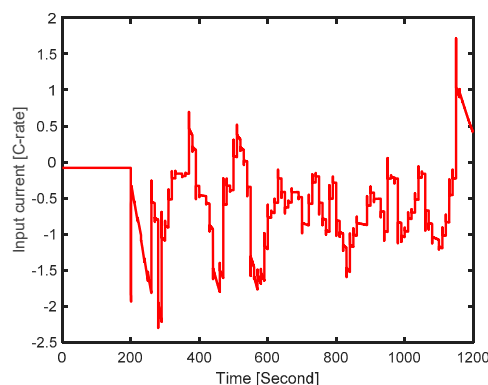
Figure 1. Input current under UDDS.
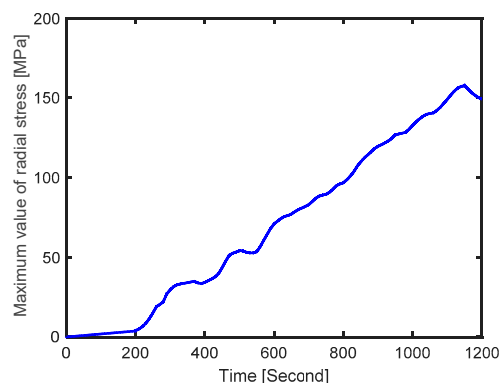
Figure 2. Maximum radial stress.
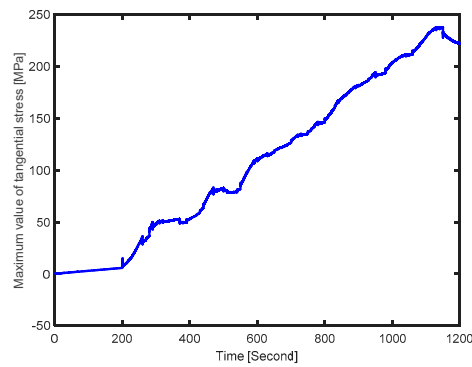
Figure 3. Maximum tangential stress.
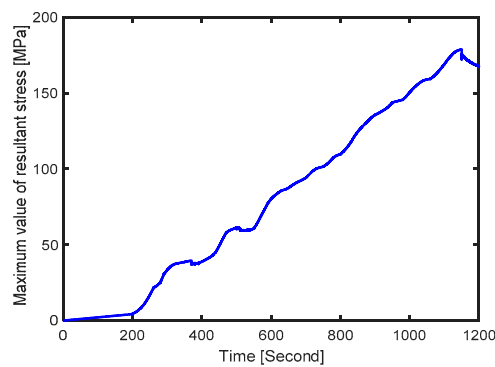
Figure 4. Maximum resultant stress.

2.3. Film Growth Model

Ramadass et al. [24] studied a resistive film formed on the anode electrode/electrolyte interphase, which is the main cause of capacity loss. The veracious chemical side reaction generating the resistive film lies on the chemical component of the anode electrode and electrolyte. Furthermore, a simplified and universal model for capacity reduction based on film growth originated from a single particle model is presented here:

$$S + Li^+ + e^- \rightarrow P \tag{22}$$

where S is the type of solvent, and P is the reaction product.

On account of this nonreversible side reaction, the reaction product builds up a film at the interface of electrode/electrolyte with a thickness varying over time $\delta_{film}(t)$. The irreversibly formed membrane together with the initial solid interphase resistance R_{SEI} forms the total resistance of the electrode/electrolyte interface as follows:

$$R_{film}(t) = R_{SEI} + \frac{\delta_{film}(t)}{\kappa_P} \tag{23}$$

where κ_p is the conductivity of the formed film.

The key state related to the increasing rate of interface film thickness, because of the unwanted lithium loss, is described by

$$\frac{\partial \delta_{film}(t)}{\partial t} = -\frac{M_P}{a_n \rho_P F} J_s(t) \tag{24}$$

where, a_n, M_p, ρ_p, and F are the formed film's specific surface area, molecular weight, mass density, and Faraday's constant, respectively. The variable $J_s(t)$ is the local volume current density used for the side reaction and described by Butler–Volmer kinetics. Assuming that the lithium reduction reaction

is nonreversible and the concentration of lithium ions in the solution changes little, it is possible to approximate $J_s(t)$ through the following equation:

$$J_s(t) = -i_{0,s}a_n e^{\left(\frac{-0.5F}{RT_{avg}}\eta_s(t)\right)}$$

(25)

where $i_{0,s}$ is current density occupied by the lithium-loss side reaction; R is the universal gas constant; and T_{avg} is the average temperature of the battery cell. The component $\eta_s(t)$ denotes the overpotential generated by the side reaction, which is expressed by the following equation:

$$\eta_s(t) = \Delta\phi(t) - U_{s,ref} - \frac{J_{tot}(t)}{a_n}R_{film}(t)$$

(26)

$$J_{tot} = J_1 + J_s$$

(27)

where $\Delta\phi(t)$ denotes the difference between the solid phase potential and electrolyte potential. The variable $U_{s,ref}$ is the reference equilibrium potential, which is considered as a constant value. The total intercalation current J_{tot} is used for the anode-side solution, which is presented by the sum of the current between the solid and solution J_1, and the solution decreasing reaction and solution J_s.

Under three different charging currents (1 C, 2 C, and 3 C), the resistance film growth rates are computed according to Equations (23)–(27) and are presented in Figure 5. From this figure, we see that the film growth rate increases as the charging current or the time increases, owing to the augmentation of the reduction reaction rate and the rise in $\Delta\phi(t)$ according to Equation (6). This means that a continuous high current and a high SoC is detrimental to reducing the lithium loss.
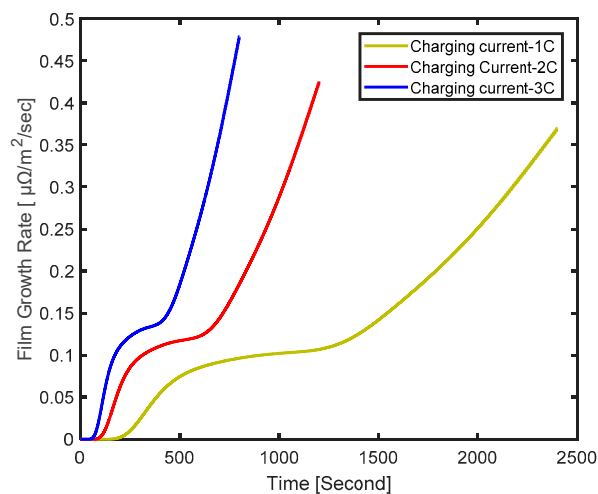
Figure 5. Film growth under three charging current.

3. Temperature Control Based on the Backstepping Technique

The core temperature of a battery cell is higher than its surface temperature, hence, the control of the core temperature being more significant. Confining the maximum temperature of the battery to a certain value can guarantee both the safe operation and efficient charging. However, the core temperature of the battery is not accessible and cannot be measured by sensor directly. Therefore, we have to estimate the core temperature of a battery cell to make sure that the control goal is achieved. H. E. Perez et al. utilized the thermal model based on the equivalent circuit model to obtain the core temperature of a battery cell, which consists of the heat conduction resistance R_c, convection resistance R_u, core heat capacity C_c, and surface heat capacity C_s [25]. The thermal model used in this paper is described by the partial differential equation, which can accurately present the evolution of spatial temperature and is more accurate than the model employed by H. E. Perez et al.

To maintain the temperature of the battery cell where we want it to be, we can adjust the temperature or flow velocity of the cooling fluid. Herein, a backstepping method is utilized to design the control law for a prespecified time-invariant reference temperature $T_{ref}(r_1)$.

The following error system is thus introduced:

$$T_e(r_1, t) = T(r_1, t) - T_{ref}(r_1), \ T_{ref}(r_1) = \frac{T_{sref} - T_{cref}}{R_b^2} r_1^2 + T_{cref} \tag{28}$$

where the expected temperature distribution $T_{ref}(r_1)$ is a quadratic parabola, which is in accordance with the true case; T_{sref} and T_{cref} are the reference surface temperature and core temperature, respectively.

The time derivative of $T_e(r_1, t)$ can be obtained according to Equations (12) and (28).

$$\begin{aligned} \frac{\partial T_e(r_1,t)}{\partial t} &= \frac{\partial T(r_1,t)}{\partial t} - \frac{\partial T_{ref}(r_1)}{\partial t} = \frac{\partial T^2(r_1,t)}{\partial r_1^2} + \frac{1}{r_1}\frac{\partial T(r_1,t)}{\partial r_1} + \frac{\dot{q}}{k} \\ &= \frac{\partial T_e^2(r_1,t)}{\partial r_1^2} + \frac{1}{r_1}\frac{\partial T_e(r_1,t)}{\partial r_1} + 2\frac{T_{sref}-T_{cref}}{R_b^2} + \frac{\dot{q}}{k} \end{aligned} \tag{29}$$

with the conditions

$$\frac{\partial T_e(0,t)}{\partial r_1} = 0, \ \frac{\partial T_e(R_b,t)}{\partial r_1} = U - 2\frac{T_{sref}-T_{cref}}{R_b}$$

where U is the boundary control law, which is applied to the boundary condition of Equation (12) for restricting $T(r_1, t)$ to around $T_{ref}(r_1)$.

Here, the following invertible backstepping transformation is adopted:

$$w(r_1, t) = T_e(r_1, t) - \int_0^{r_1} K(r_1, \rho) T_e(\rho, t) d\rho \tag{30}$$

which maps (29) into the stable system:

$$w_t = w_{r_1 r_1} + \frac{w_{r_1}}{r_1} - \frac{cw}{r_1^2} \tag{31}$$

with boundary conditions

$$w_{r_1}(0, t) = 0, w_{r_1}(R_b, t) = 0 \tag{32}$$

where $c > 0.5$. $K(r_1, \rho)$ can be solved easily by the following kernel function:

$$K_{r_1 r_1} + \frac{K_{r_1}}{r_1} - K_{\rho\rho} + \frac{K_\rho}{\rho} - \frac{K}{\rho^2} = \frac{c}{r_1^2} K \tag{33}$$

with the following conditions:

$$K(r_1, 0) = 0, \ K_\rho(r_1, 0) = 0, \ K(r_1, r_1) = -\int_0^r \frac{c/r_1^2}{2} d\rho \tag{34}$$

The detailed solution process can be seen in [26].

According to the boundary condition $w_{r_1}(R_b, t) = 0$ and Equation (29), we have

$$\frac{\partial T_e(R_b,t)}{\partial r_1} = K(R_b, R_b)T_e(R_b, t) + \int_0^{R_b} K_{r_1}(R_b, \rho)T_e(\rho, t) d\rho \tag{35}$$

Then, the control law is obtained:

$$U = K(R_b, R_b)T_e(R_b, t) + \int_0^{R_b} K_{r_1}(R_b, \rho)\big[T(\rho, t) - T_{ref}(\rho)\big]d\rho + 2\frac{T_{sref} - T_{cref}}{R_b} \tag{36}$$

The control law requires access to the full states $T(\rho, t)$. However, the core temperature cannot be measured by sensor directly. For that, the following boundary temperature observer is proposed:

$$\frac{\partial \hat{T}(r_1, t)}{\partial t} \frac{1}{\alpha} = \frac{\partial \hat{T}^2(r_1, t)}{\partial r_1^2} + \frac{1}{r_1} \frac{\partial \hat{T}(r_1, t)}{\partial r_1} + \frac{\dot{q}}{k} + P(r_1)(T(R_b, t) - \hat{T}(R_b, t)) \tag{37}$$

with boundary conditions

$$\frac{\partial \hat{T}(0, t)}{\partial r_1} = 0, \frac{\partial \hat{T}(R_b, t)}{\partial r_1} = U = \frac{h}{k}(T_a - T(R_b, t))$$

The estimation error $\widetilde{T}(r_1, t) = T(r_1, t) - \hat{T}(r_1, t)$ is introduced, then substituting Equation (37) for Equation (12), one has

$$\frac{\partial \widetilde{T}(r_1, t)}{\partial t} \frac{1}{\alpha} = \frac{\partial \widetilde{T}^2(r_1, t)}{\partial r_1^2} + \frac{1}{r_1} \frac{\partial \widetilde{T}(r_1, t)}{\partial r_1} - P(r_1)(\widetilde{T}(R_b, t)) \tag{38}$$

with boundary conditions

$$\frac{\partial \widetilde{T}(0, t)}{\partial r_1} = 0, \frac{\partial \widetilde{T}(R_b, t)}{\partial r_1} = 0$$

Using the following backstepping transform, which is similar with (30), we have

$$w(r_1, t) = \widetilde{T}(r_1, t) - \int_0^{r_1} M(r_1, \rho)\widetilde{T}(\rho, t)d\rho \tag{39}$$

where $w(r_1, t)$ satisfies the following stable system:

$$w_t = w_{r_1 r_1} + \frac{w_{r_1}}{r_1} - \frac{dw}{r_1^2} \tag{40}$$

with boundary conditions

$$w_{r_1}(0, t) = 0, w_{r_1}(R_b, t) = 0$$

where $d > 0.5$ as well. $M(r_1, \rho)$ satisfies the following kernel function:

$$M_{r_1 r_1} + \frac{M_{r_1}}{r_1} - M_{\rho\rho} + \frac{M_\rho}{\rho} - \frac{M}{\rho^2} = -\frac{c}{r_1^2}M \tag{41}$$

with the boundary conditions:

$$M_\rho(0, \rho) = 0, M(r_1, r_1) = -\int_0^{r_1} \frac{c/r_1^2}{2}d\rho$$

The solution procedure of $M(r_1, \rho)$ is similar to $K(r_1, \rho)$.

To verify the performance of the backstepping-based observer and controller, a constant current of 2 C is applied to a battery cell; the curve of the temperature rising is presented in Figure 6. $r = 0$ and $r = 1$ represent the center and the surface of a battery cell, respectively. The two horizontal lines are the target temperature of the surface and the center of a battery cell. From Figure 6, we can see that the temperature estimation of both the surface and the center is capable of tracking the true temperature and approaching the target temperature gradually. That is to say that we can control the temperature to a safe range using the proposed temperature controller.
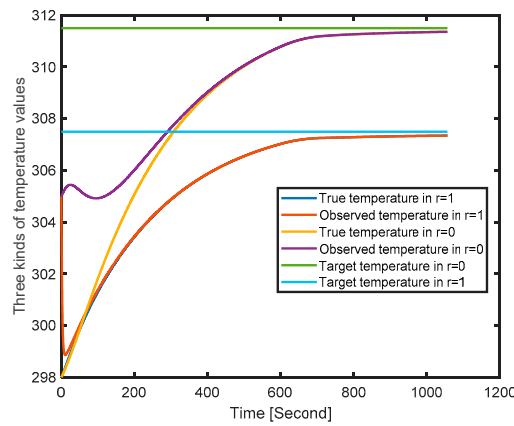
Figure 6. Estimation and control of temperature.

4. Problem Formulation

This paper concentrates on the minimization of the charging time in a given target SoC with limits involving current, voltage, intercalation-induced stress, and film formation. The simultaneous nonlinear programming approach is used in this paper. Considering the optimal charging profile with predetermined final SoC under the objective of minimization of charging time, the objective function J is given by

$$J = \min_{I(t),s(t),t_f} \int_{t_0}^{t_f} 1 \cdot dt \tag{42}$$

with bounds

$$I_{\min} \leq I(t) \leq I_{\max} \tag{43}$$

$$t_0 \leq t_f \leq t_{\max} \tag{44}$$

$$V_{\min}(t) \leq V(t) \leq V_{\max}(t) \tag{45}$$

$$\sigma_{r,\max}^-(t) \leq \sigma_{r,\text{upper}}^- \tag{46}$$

$$-\sigma_{t,\max}^-(t) \leq \sigma_{t,\text{upper}}^- \tag{47}$$

$$\partial \dot{\delta}_{film}(t) \leq \partial \dot{\delta}_{film\_\max}(t) \tag{48}$$

where $I(t)$ is the input current (A); t_f is the final time (s); $V(t)$ is the terminal voltage (V); $\sigma_{r,\text{upper}}^-(t)$ and $\sigma_{t,\text{upper}}^-$ are the radial and tangential stress upper bounds, respectively; and $\partial \dot{\delta}_{film\_\max}(t)$ is the upper bound of the film growth rate.

5. Simulation and Results

In order to verify the performance of the proposed optimal fast-charging method, CC–CV, the most common pattern of fast charging, was used for the comparative study, including four aspects: charging time, maximum tangential stress, maximum radial stress, and film growth rate.

In the process of fast charging a lithium battery, the temperature of the battery cell grows quickly and the aging rate increases. To avoid overheating, the backstepping method is used to keep the battery cell at a constant temperature, as shown in Figure 7. A constant temperature in the battery cell not only helps avoid overheating, but also helps compare the performance of the proposed fast-charging method with the CC–CV method. In order to find a compromise between the charging time and battery aging, the proposed optimal fast-charging method in this paper considers two aging factors: intercalation-induced stress and film growth. In the comparative study, the CC–CV pattern adopts three kinds of maximum charging current: 1 C, 2 C, and 3 C. This means that the effect of the choice of the maximum charging current on the comparative results is avoided.

In this paper, the upper limits of the radial and tangential stress are predetermined and optimal charging curves were obtained using the dynamic optimization approach. As we know, when charging occurs, the maximum tangential stress is located at the surface of the particle, and the maximum radial stress is located at the center of the particle. For an anode made of graphite, neither the maximum tangential stress nor the maximum radial stress is not allowed to exceed the yielding stress for any length of time to reduce the risk of anode fracture. The following case is discussed: charging a battery from 0% SoC to 100% SoC.
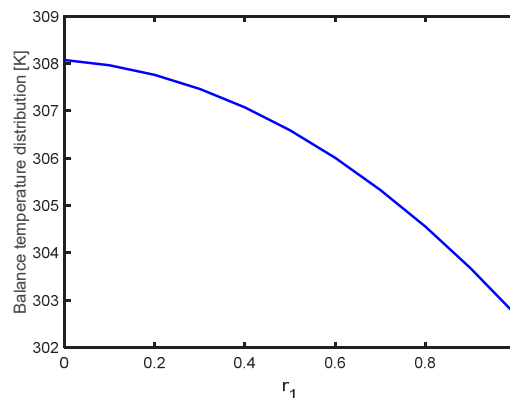
Figure 7. The balance temperature distribution.

Figure 7 presents the balance of temperature distribution. If this balance is broken, the temperature controller would work to drag the temperature to the target position using various methods, such as changing the fluid temperature and adjusting the fluid flow velocity. Thus, a stable cell temperature can be achieved for safe operation. Figures 8 and 9 show the current and voltage curves of charging a battery from 0% SoC to 100% SoC by utilizing the CC–CV pattern under three maximum charging currents. At the initial charging stage, the input current maintains at the maximum and the terminal voltage climbs fast. When the output voltage reaches the upper value, this voltage is held until the battery cell is charged fully. With the increase in the maximum charging current, the time cost for full charging becomes less and less. Figure 10 indicates the optimal charging current obtained by the dynamic optimization method. The upper value and lower values of the constraints are listed in Table 1.
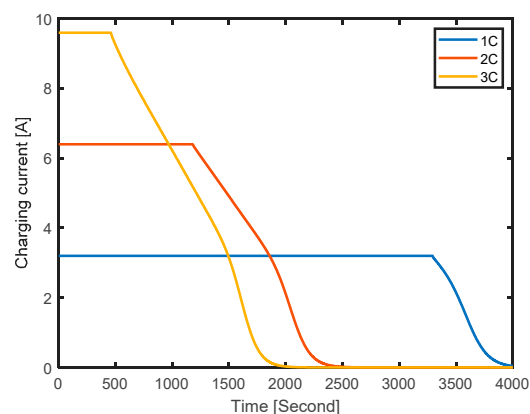
Figure 8. Three Current profiles under CC–CV.
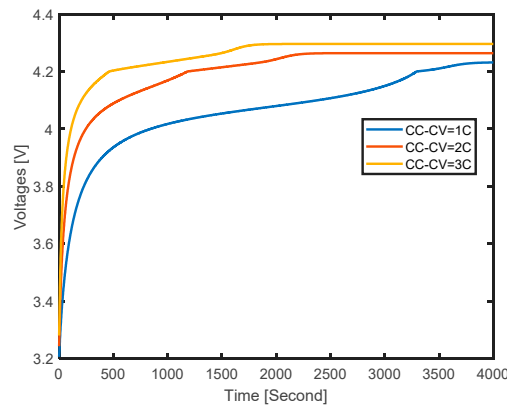
Figure 9. Corresponding voltages under CC–CV.
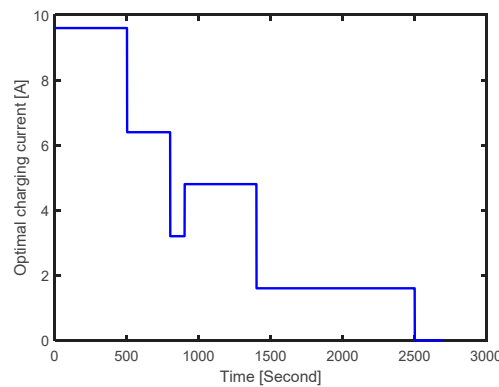
Figure 10. Optimal charging profile.

Table 1. The upper value or lower values of the constraints.

Range	$I(t)$ (C)	t_f (min)	$V(t)$ (V)	$\sigma^-_{r,\mathbf{max}}(t)$ (MPa)	$-\sigma^-_{t,\mathbf{max}}(t)$ (MPa)	$\partial\dot{\delta}_{film}(t)$ (μΩ/m²/s)
Upper	3	80	4.3	160	220	0.5
Lower	0	15	2	0	0	0

From Figure 11, we see that the area under the film growth curve is smaller than those of the other three curves, which means the least lithium loss during full charging. At the same time, the charging time of the optimal charging profile just takes 200 s more than the time cost under CC–CV with a 3 C current, which is fast enough and acceptable.
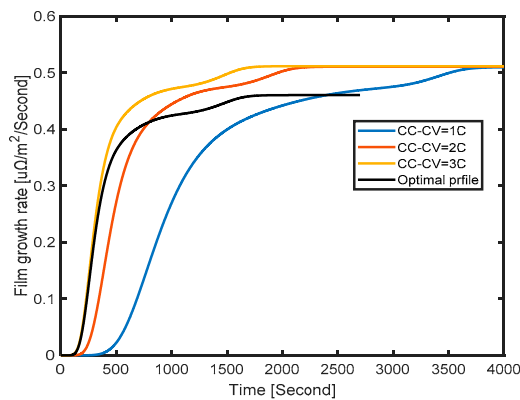
Figure 11. Film growth rate under four profiles.

The yielding stress of the radial stress and tangential stress in a graphite-based anode are both around 30 MPa. If the radial stress or tangential stress is more than 30 Mpa for a long time, it is possible to cause fatigue failure and accelerate the aging process. From Figure 12, the tangential stress generated by optimal charging profile becomes greater than its yielding stress within 1400 s, while the tangential stress under CC–CV with 1 C, 2 C, and 3 C is larger than 30 MPa for more than 1700 s, 2200 s, and 3700 s, respectively. From the maximum values of radial stress as shown in Figure 13, we can see that the optimal charging profile causes a shorter period of overstress, which represents less electrode fatigue damage. Hence, the result shows that the optimal charging profile obtained by the dynamic optimization method has less probability of causing stress than the CC–CV profiles and so can slow the aging process and extend the battery life.
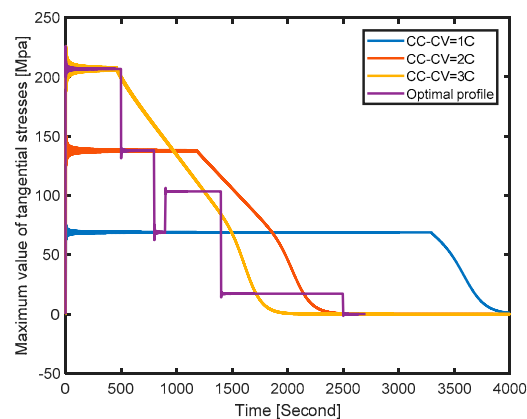
Figure 12. Maximum value of tangential stress.
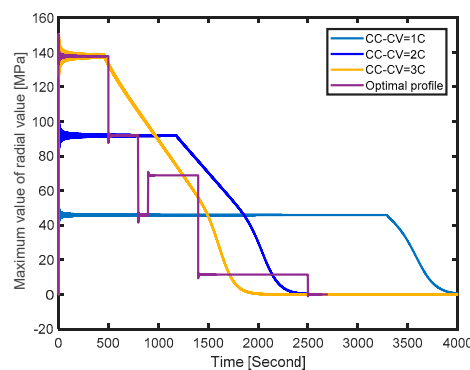
Figure 13. Maximum value of radial stress.

Therefore, while optimizing the charging speed, the proposed optimal charging method offers a good compromise between charging time and battery aging.

6. Conclusions

In this paper, the electrochemical–thermal model was employed to obtain the optimal charging profile and control the temperature of the cell. A temperature controller-based backstepping method was proposed to keep a relatively constant cell temperature to avoid overheating. Then, the effects of intercalation-induced stress were considered, because these cause particle fracture, which can accelerate the aging process. Furthermore, the growth of film on the surface of particles was also taken into account due to its ability to reduce the reused lithium ions. After that, the optimization objective was established, which minimizes the time cost during charging, while confining intercalation-induced stress and the growth rate of surficial film to a given range. Finally, the simulation was implemented and the results show that the film growth of the optimal charging curve is smaller than that of the other

three charging curves, thus demonstrating the least lithium loss during full charging. Besides that, the tangential stress and the radial stress generated by the optimal charging profile were both greater than their yielding stresses for less time during charging as compared with the CC–CV pattern, which means there is less risk of electrode fatigue fracture. Furthermore, the charging time of the optimal charging profile just takes 200 s more than the time cost under CC–CV with a 3 C current, which is fast enough and acceptable. Hence, the proposed optimal charging method offers a good compromise between charging time and battery aging.

Abbreviations

The following abbreviations are used in this manuscript:

BMS	Batteries management system
DP	Dynamic optimization
SoC	State of Charge
CC-CV	Constant current-constant voltage
CC	Constant current
IC	Incremental capacity
OCV	Open circuit voltage
TTC	Time-to-charge
EL	Energy losses
TRI	Temperature rise index
P2D	Pseudo-two dimensional
MPC	Model predictive control
CT-CV	Constant temperature-constant voltage
LGR	Legendre-Gauss-Radau
PID	Proportional-integral-derivative
SPM	Single particle model
PDE	Partial differential equation
ODE	Ordinary differential equation
UDDS	Urban Dynamometer Driving Schedule

References

1. Dehghani-Sanij, A.; Tharumalingam, E.; Dusseault, M.; Fraser, R. Study of energy storage systems and environmental challenges of batteries. *Renew. Sustain. Energy Rev.* **2019**, *104*, 192–208. [CrossRef]
2. Liu, Y.; Luo, Y. Search for an Optimal Rapid-Charging Pattern for Li-Ion Batteries Using the Taguchi Approach. *IEEE Trans. Ind. Electron.* **2010**, *57*, 3963–3971. [CrossRef]
3. Abdollahi, A.; Raghunathan, N.; Han, X.; Avvari, G.V.; Balasingam, B.; Pattipati, K.R.; Bar-Shalom, Y. Battery Charging Optimization for OCV-Resistance Equivalent Circuit Model. In Proceedings of the 2015 American Control Conference Palmer House Hilton, Chicago, IL, USA, 1–3 July 2015.
4. Abdollahi, A.; Han, X. Optimal battery charging, Part I: Minimizing time-to-charge, energy loss, and temperature rise for OCV-resistance battery model. *J. Power Sources* **2016**, *303*, 388–398. [CrossRef]
5. Monem, M.A.; Trad, K.; Omar, N.; Hegazy, O.; Mantels, B.; Mulder, G.; Bossche, P.V.D.; Van Mierlo, J. Lithium-ion batteries: Evaluation study of different charging methodologies based on aging process. *Appl. Energy* **2015**, *152*, 143–155. [CrossRef]

6. Liu, K.; Li, K.; Yang, Z.; Zhang, C.; Deng, J. An advanced Lithium-ion battery optimal charging strategy based on a coupled thermoelectric model. *Electrochim. Acta* **2017**, *225*, 330–344. [CrossRef]

7. Fang, H.Z.; Wang, Y.B.; Chen, J. Health-Aware and User-Involved Battery Charging Management for Electric Vehicles: Linear Quadratic Strategies. *IEEE Trans. Control Syst. Technol.* **2017**, *25*, 911–923. [CrossRef]

8. Patnaik, L.; Praneeth, A.V.J.S.; Williamson, S.S. A Closed-Loop Constant-Temperature Constant-Voltage Charging Technique to Reduce Charge Time of Lithium-Ion Batteries. *IEEE Trans. Ind. Electron.* **2019**, *66*, 1059–1067. [CrossRef]

9. Klein, R.; Chaturvedi, N.A.; Christensen, J.; Ahmed, J.; Findeisen, R.; Kojic, A. Optimal charging strategies in lithium-ion battery. In Proceedings of the 2011 American Control Conference, San Francisco, CA, USA, 29 June–1 July 2011. [CrossRef]

10. Pramanik, S.; Anwar, S. Electrochemical model based charge optimization for lithium-ion batteries. *J. Power Sources* **2016**, *313*, 164–177. [CrossRef]

11. Perez, H.E.; Dey, S.; Hu, X.; Moura, S.J. Optimal Charging of Li-Ion Batteries via a Single Particle Model with Electrolyte and Thermal Dynamics. *J. Electrochem. Soc.* **2017**, *164*, A1–A9. [CrossRef]

12. Anseán, D.; Gonzalez, M.; Viera, J.C.; García, V.; Blanco, C.; Valledor, M. Fast charging technique for high power lithium iron phosphate batteries: A cycle life analysis. *J. Power Sources* **2013**, *239*, 9–15. [CrossRef]

13. Anseán, D.; Dubarry, M.; Devie, A.; Liaw, B.Y.; García, V.; Viera, J.; Gonzalez, M. Fast charging technique for high power LiFePO4 batteries: A mechanistic analysis of aging. *J. Power Sources* **2016**, *321*, 201–209. [CrossRef]

14. Suthar, B.; Ramadesigan, V.; De, S.; Braatz, R.D.; Subramanian, V.R. Optimal charging profiles for mechanically constrained lithium-ion batteries. *Phys. Chem. Chem. Phys.* **2014**, *16*, 277–287. [CrossRef] [PubMed]

15. Torchio, M.; Magni, L.; Braatz, R.; Raimondo, D.M. Optimal Health-aware Charging Protocol for Lithium-ion Batteries: A Fast Model Predictive Control Approach. In Proceedings of the International Federation of Automatic Control, Sherbrooke, QC, Canada, 21–25 August 2016.

16. Abdel-Monem, M.; Trad, K.; Omar, N.; Hegazy, O.; Bossche, P.V.D.; Van Mierlo, J. Influence analysis of static and dynamic fast-charging current profiles on ageing performance of commercial lithium-ion batteries. *Energy* **2017**, *120*, 179–191. [CrossRef]

17. Umair Ali, M.; Hussain Nengroo, S.; Adil Khan, M.; Zeb, K.; Ahmad Kamran, M.; Kim, H.J. A Real-Time Simulink Interfaced Fast-Charging Methodology of Lithium-Ion Batteries under Temperature Feedback with Fuzzy Logic Control. *Energies* **2018**, *11*, 1122. [CrossRef]

18. Wang, Y.; Hu, X.; Wei, Z.; Wik, T.; Egardt, B. Electrochemical Estimation and Control for Lithium-Ion Battery Health-Aware Fast Charging. *IEEE Trans. Ind. Electron.* **2018**, *65*, 6635–6645.

19. Lin, X.; Hao, X.; Liu, Z.; Jia, W. Health conscious fast charging of Li-ion batteries via a single particle model with aging mechanisms. *J. Power Sources* **2018**, *400*, 305–316. [CrossRef]

20. Xu, M.; Wang, R.; Zhao, P.; Wang, X. Fast charging optimization for lithium-ion batteries based on dynamic programming algorithm and electrochemical-thermal-capacity fade coupled model. *J. Power Sources* **2019**, *438*, 15–27. [CrossRef]

21. Moura, S.J.; Argomedo, F.B.; Klein, R.; Mirtabatabaei, A.; Krstic, M. Battery State Estimation for a Single Particle Model with Electrolyte Dynamics. *EEE Trans. Control Syst. Technol.* **2016**, *25*, 453–468. [CrossRef]

22. Zhang, D.; Dey, S.; Couto, L.D.; Moura, S.J. Battery Adaptive Observer for a Single Particle Model with Intercalation-Induced Stress. *IEEE Trans. Control. Syst. Technol.* **2019**, 1–15. [CrossRef]

23. Zhang, X.C.; Shyy, W.; Sastrya, A.M. Numerical Simulation of Intercalation-Induced Stress in Li-Ion Battery Electrode Particles. *J. Electrochem. Soc.* **2007**, *154*, A910–A916. [CrossRef]

24. Ramadass, P.; Haran, B.; Gomadam, P.M.; White, R.; Popov, B.N. Development of first principles capacity fade model for Li-ion cells. *J. Electrochem. Soc.* **2004**, *151*, 196–203. [CrossRef]

25. Perez, H.E.; Hu, X.; Dey, S.; Moura, S. Optimal Charging of Li-Ion Batteries with Coupled Electro-Thermal-Aging Dynamics. *IEEE Trans. Veh. Technol.* **2017**, *66*, 7761–7770. [CrossRef]

26. Vazquez, R.; Krstic, M. Boundary control and estimation of reaction–diffusion equations on the sphere under revolution symmetry conditions. *Int. J. Control* **2019**, *92*, 2–11. [CrossRef]